Composites Part B 216 (2021) 108806

Contents lists available at ScienceDirect

Composites Part B

journal homepage: www.elsevier.com/locate/compositesb

Design optimization of double-layered structural insulated panels for windborne debris hazard

Dikshant Saini [a], Behrouz Shafei [a,b,*]

[a] Department of Civil, Construction, and Environmental Engineering, Iowa State University, Ames, IA, 50011, United States
[b] Department of Materials Science and Engineering, Iowa State University, Ames, IA, 50011, United States

ARTICLE INFO

Keywords:
Double-layered structural insulated panels
Windborne debris hazard
Impact simulations
Global sensitivity analysis
Multi-objective design optimization

ABSTRACT

The design and performance of double-layered structural insulated panels (DL-SIPs) are investigated in this study with a focus on how they resist the windborne debris hazard. Such composite panels are commonly used in building envelopes to provide insulation and energy-saving advantages. However, if not designed properly, they can be at the risk of failure due to windborne debris impact, especially in high wind regions. This critical aspect motivated the current study to establish an experimentally-supported computational platform to assess the DL-SIPs, in terms of their key response measures, such as energy absorption, maximum displacement, and projectile penetration. A global sensitivity analysis is then conducted to systematically evaluate the effects of various design variables considered for metal sheets and foam cores on the impact response characteristics of the DL-SIPs. This study is further extended to perform a multi-objective design optimization for the DL-SIPs using two surrogate models (i.e., radial basis function network and kriging model). From the optimization results, the trade-offs between the design details and the impact resistance measures are determined. This leads to a set of configurations recommended for the DL-SIPs to properly resist windborne debris impact, while avoiding an overdesign.

1. Introduction

During strong winds, such as hurricanes and tornadoes, building envelopes are at a major risk to experience damage from windborne debris impact. Depending on the impact's intensity, the debris can partially penetrate or even cause perforation in the building envelopes, leading to severe safety and performance concerns. To achieve a safe design of the building envelopes in the regions prone to the windborne debris hazard, a set of guidelines and standards have been developed to test the panels used as exterior walls [1–4]. Among various exterior wall alternatives available for residential and commercial buildings, structural insulated panels (SIPs) have become a popular choice, primarily because they offer a large rigid panel, providing excellent insulation and energy-saving advantages. A typical SIP consists of foam materials, such as expanded polystyrene (EPS) and extruded polystyrene (XPS), sandwiched between two structural skins. The structural skins can be made of various materials, including galvalume/zincalume steel, fiber-reinforced cement, and fiberglass. Depending on the target application, the SIP can have a thickness in the range between 50 mm (2 in) and 300 mm (12 in).

In the existing literature, only a limited number of studies are available with a focus on the performance of SIPs against the windborne debris hazard [5–11]. Among them, Chen et al. [5,9,10] investigated the SIPs under impact loads and reported that the panels with ductile face sheets can experience (relatively) large deformations if not designed properly. In a separate study, Saini and Shafei [12] examined the perforation resistance of the SIPs made with metal skins. The investigations led to the development of vulnerability curves to predict the risk of failure of the SIPs under debris impact. Departing from single-layered configurations, multi-layered SIPs have also been explored in the literature [13–20]. Zhou and Stronge [14] performed ballistic tests on such panels and revealed how the layered placement of multiple plates enhanced the energy absorption capacity compared to a single-layer plate of the same total thickness. Focusing on the sandwich panels with layered cores, Jing et al. [15] investigated how the inclusion of multiple cores can help the impact resistance of sandwich panels. In another study on multi-layered panels, Sun et al. [16] evaluated the impact response of sandwich panels with homogenous and stepwise graded foam cores. The study reported that the perforation resistance of the panels can be improved by increasing the density of the first foam

* Corresponding author. Department of Civil, Construction, and Environmental Engineering, Iowa State University, Ames, IA, 50011, United States.
E-mail addresses: dikshant@iastate.edu (D. Saini), shafei@iastate.edu (B. Shafei).

https://doi.org/10.1016/j.compositesb.2021.108806
Received 4 December 2020; Received in revised form 8 March 2021; Accepted 15 March 2021
Available online 26 March 2021

core.

Despite the promise of multi-layered sandwich panels, the relevant literature does not provide the fundamental insights necessary for their design and implementation, especially where the risk of windborne debris impact is significant. This motivated the current study to address the existing research gaps with a focus on double-layered structural insulated panels (DL-SIPs). To offer a holistic perspective, an experimentally-supported computational platform is developed, in conjunction with a rigorous optimization framework. For the computational platform, a set of finite-element (FE) models representative of DL-SIPs are generated. Upon validating the developed FE models using the experimental test results, the impact response of the modeled DL-SIPs is characterized, in terms of key performance measures, such as energy absorption, maximum displacement, and projectile penetration. A global sensitivity analysis is then conducted for evaluating the effects of main design variables, including the geometric and material properties of metal sheets and foam cores, on the impact response of DL-SIPs. After obtaining a detailed understanding of the extent of contribution of various design variables, a multi-objective design optimization (MDO) is conducted using two surrogate models, i.e., radial basis function (RBF) network and kriging model. The MDO spans three scenarios to capture the trade-offs among the energy absorption, maximum displacement, and projectile penetration measures extracted for a total of 120 design combinations. The outcome of this study helps researchers, engineers, and practitioners move toward optimizing the design of DL-SIPs used in building envelopes, especially to mitigate the risk of the windborne debris hazard.

2. Details of DL-SIP models subjected to debris impact

In this study, the DL-SIPs are modeled with all the necessary details using LS-DYNA [21]. The main response characteristics are then investigated under windborne debris impact with a wide range of velocities. In this section, a detailed description of the FE models of the DL-SIPs, including their geometric details, material models, contact algorithms, and loading scenarios, is provided.

2.1. Model setup

The current study investigates the DL-SIPs that represent the composite wall panels commonly used in the building envelopes. The modeled DL-SIPs consist of two foam cores sandwiched between three metal sheets, as shown in Fig. 1. The base DL-SIP models have the in-plane dimensions of 1.2 m × 2.4 m and the thickness of 50 mm for each core. The metal sheets are 0.4-mm thick zincalume G300 steel, similar to those studied in the past [8,10,12]. To model these thin metal sheets, fully-integrated shell elements with five through thickness integration points are employed. For the foam core, EPS is used, owing to its excellent energy absorption capacity. Constant stress solid elements (with eight nodes) are employed to model the foam cores. To investigate the resistance of DL-SIPs to windborne debris impact, large missile tests prescribed by Florida Building Code [4] for extreme conditions are employed. In such tests, a wood sawn lumber with the cross-sectional dimensions of 50 mm × 100 mm (2 in. × 4 in.) and the mass of 4.1 kg (8.8 lb) is used as the test missile.

2.2. Material models for metal sheets and foam cores

The mechanical properties of the zincalume G300 steel sheets in the DL-SIPs are adopted from the past studies [10,12]. The metal sheets have the Young's modulus and Poisson's ratio of 210 GPa and 0.3, respectively. To capture the nonlinear behavior of the steel sheets, a yield stress and a failure strain of 330 MPa and 0.0525 are defined, respectively. The constitutive behavior of the steel is defined using the elastic-plastic material model with kinematic hardening and strain rate effects. Similar to previous studies [22–26], Cowper and Symonds model [27] is utilized to model the strain rate effects. This model is expressed using the following equation:

$$\frac{\sigma_d}{\sigma_s} = 1 + \left(\frac{\dot{\varepsilon}}{C}\right)^{\frac{1}{p}} \tag{1}$$

where σ_d and σ_s are the dynamic flow stress and the associated flow stress, respectively; $\dot{\varepsilon}$ is the strain rate; and C and p are the model parameters assumed as 100 s^{-1} and 10, respectively [10].

The EPS foam with various densities are considered in the current study for the foam core. Under external loads, the EPS foam is known to exhibit three different response characteristics, which can be categorized to elastic, compaction, and densification regions. The EPS foam under compression provides a linear elastic response, followed by a distinct plateau and final densification, as the applied strain increases. It is important to note that the yield strength and elastic modulus of the EPS foam under compression directly depends on its density. To model

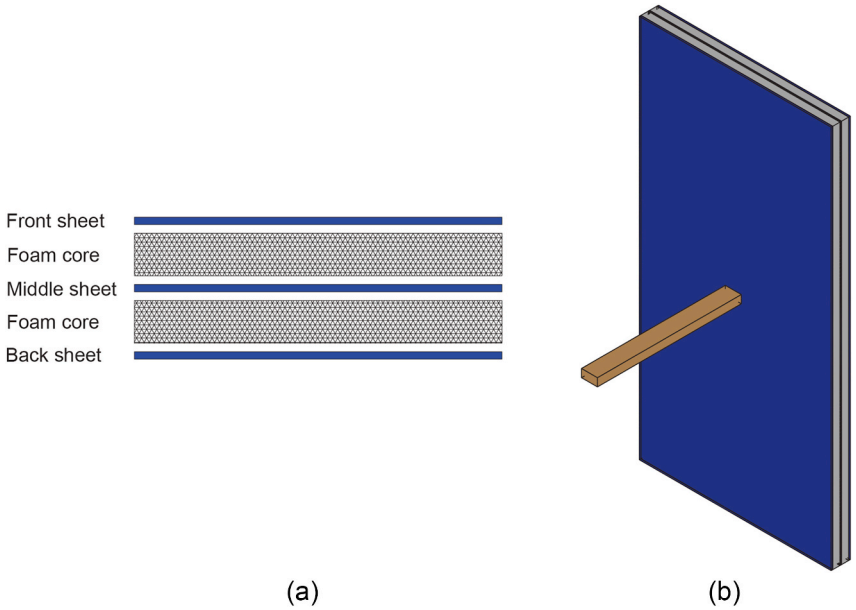

Fig. 1. Details of the base DL-SIP developed for the windborne debris impact simulations: (a) cross-sectional view, and (b) overall setup.

the EPS foam under impact loads, the crushable foam models are deemed appropriate, due to their efficiency in capturing such foam's crushing behavior. The current study employs the modified crushable foam model, which assumes that the foam is isotropic. The strain rate effects are accounted by defining the stress-volumetric strain curves for different strain rates. The material model captures the stress in the model based on the volumetric strain and volumetric strain rate. To introduce the stress-strain curves of the EPS foams with various densities, the empirical model developed by Avalle et al. [28] is used, based on the following equation:

$$\sigma = A\left(1 - e^{(-E/A)\varepsilon(1-\varepsilon)^m}\right) + B\left(\frac{\varepsilon}{1-\varepsilon}\right)^n \tag{2}$$

where σ and ε are the engineering stress and strain, respectively; and E, A, and B are the stress-strain parameters that depend on the foam density, ρ. In the SIPs, the EPS foams sandwiched between the metal sheets are highly compressible and have a very small Poisson's ratio (~0.0001). Therefore, although Equation (2) is for a one-dimensional (1D) stress-strain state, it can closely approximate the stress versus volumetric strain behavior of the modeled foams. The following equations are employed to obtain the stress-strain parameters:

$$E = 1.094 \times 10^{-1}\rho \tag{3}$$

$$A = 7.551 \times 10^{-3}\rho + 4.063 \times 10^{-4}\rho^{3/2} \tag{4}$$

$$B = 5.880 \times 10^{-4}\rho^{1.388} \tag{5}$$

In the original form of Equation (2), the m and n parameters had been assumed independent of the density of the EPS foam. This assumption led to the deviation of the plateau compaction region of the stress-strain curve from that recorded during the experiments. This has been resolved by modeling both parameters as a function of the EPS foam density. To model the EPS foam under impact loads, the empirical dynamic increase factor (*DIF*) equations provided by Chen et al. [29] are used:

$$DIF = 1.144 + 0.045\log(\dot{\varepsilon}) \text{ for } 10^{-3} < \dot{\varepsilon} < 113 \tag{6}$$

$$DIF = -0.157 + 0.680\log(\dot{\varepsilon}) \text{ for } \dot{\varepsilon} \geq 113 \tag{7}$$

Fig. 2 compares the stress-strain relationship of 61.0 kg/m^3 density EPS foam obtained from the model (under two strain rates of 0.0087 s^{-1} and 1371 s^{-1}) to the experimental test results [30]. It is observed that the empirical model closely captures the mechanical characteristic of the EPS foam. Noting that the crushable foam model is incapable of modeling the element erosion in the foam, a shear strain failure criterion with a maximum shear strain of 0.5 is included to properly simulate the process of damage formation and propagation in the EPS foam. The wood lumber projectile is modeled in this study with a rigid material based on the fact that it often undergoes no notable deformation/degradation upon impact. After confirming that the elastic energy absorbed by the lumber projectile is negligible compared to the energy absorbed by the DL-SIPs, this assumption was concluded to maintain the expected accuracy, while reducing the computational time.

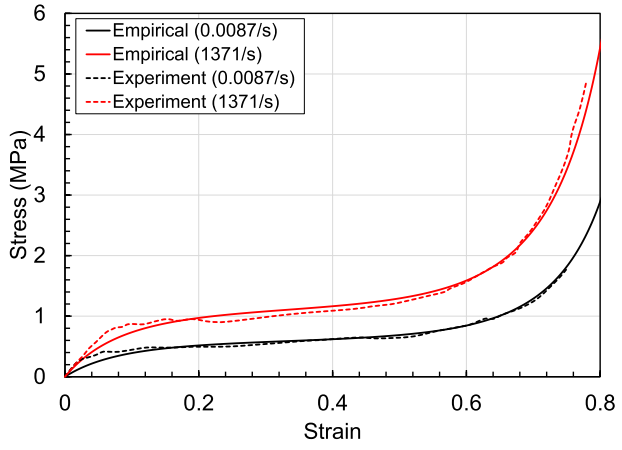

Fig. 2. Comparison of the stress-strain relationship of the EPS foam (with the density of 61.0 kg/m^3) obtained from the empirical model and conducted experiments [30] under two strain rates.

2.3. Support conditions and contact details

In the current construction practice, an individual panel cannot cover the entire wall, and thus, a pair of them are installed side by side with a connection. As a result, three edges of each panel have a fixed boundary condition, while the fourth edge has a partially-fixed boundary condition, i.e., the out-of-plane movement is not fully constrained. For real-world applications, the actual boundary condition of the fourth edge of DL-SIPs depends on its connection details, which provide constraints in a range between partially-fixed and fully-fixed boundary conditions. From a set of preliminary investigations, it has been found that the level of edge fixity has a negligible effect on the key impact response measures of DL-SIPs. Thus, the modeled DL-SIPs are considered to be fixed along all the four edges. This is achieved by applying single-point constraints on all the four edges of the panel. When a windborne debris impacts a DL-SIP, its kinetic energy is known to be transferred to various components of the DL-SIP. To fully capture the interactions between the panel components, an eroding surface-to-surface contact with a scaled penalty stiffness is employed [31,32]. An interior contact is also included to prevent a negative volume error. In the impact tests conducted on the SIPs, the metal sheets and the foam cores were found to remain bonded throughout the entire experiment [10]. Thus, the common nodes of the metal sheets and the foam cores are merged in the FE models.

3. Validation of developed simulation platform

Before advancing to the main impact simulations, the developed computational platform is validated using the experimental test results. The first set of validations involves the impact tests on the EPS foam. Zhang et al. [33] performed quasi-static, dynamic, and indentation tests on the EPS foams. The test setup consists of a square EPS foam block (with the in-plane dimensions of 200 m × 200 mm and the thickness of 60 mm), resting on a rigid steel plate. For the impact load, a 77.9 kg drop hammer with a hemispherical nose is released from a height of 3.262 m. To verify the modeling details of the EPS foam, two EPS foam specimens with the densities of 13.0 kg/m^3 and 18.0 kg/m^3 are investigated. For each of the two foam specimens, the impact force and displacement time-histories are extracted from the FE simulations and compared to those recorded during the experiments. As reflected in Fig. 3, the simulations are found to capture both peak impact force and impact duration closely. Further to impact forces and durations, the simulations provide a close replication of the displacement response, confirming that the modified crushable foam model captures the response of the EPS foam to impact loads.

In the absence of any experimental tests on the windborne debris impact response of DL-SIPs, the current study utilizes the experimental test results available for single-layered SIPs [10]. This includes a diverse set of six single-layered SIP simulations that represent the details similar to those used in the DL-SIPs. The SIPs under consideration consist of an EPS foam core and two zincalume G300 steel sheets with the in-plane dimensions of 1200 mm × 762 mm. The wood lumber that has a mass of 4.1 kg is launched using a pneumatic canon. In this study, the SIPs were subjected to several impact velocities starting from 17.0 m/s to 26.0 m/s. The metal sheets used in the investigated SIPs have a yield strength of 330 MPa and a thickness of 0.42 mm. The tested single-layered SIPs have three different core thicknesses, ranging from 38 mm to 75 mm, with a density of 13.5 kg/m^3. The edges of the SIPs are

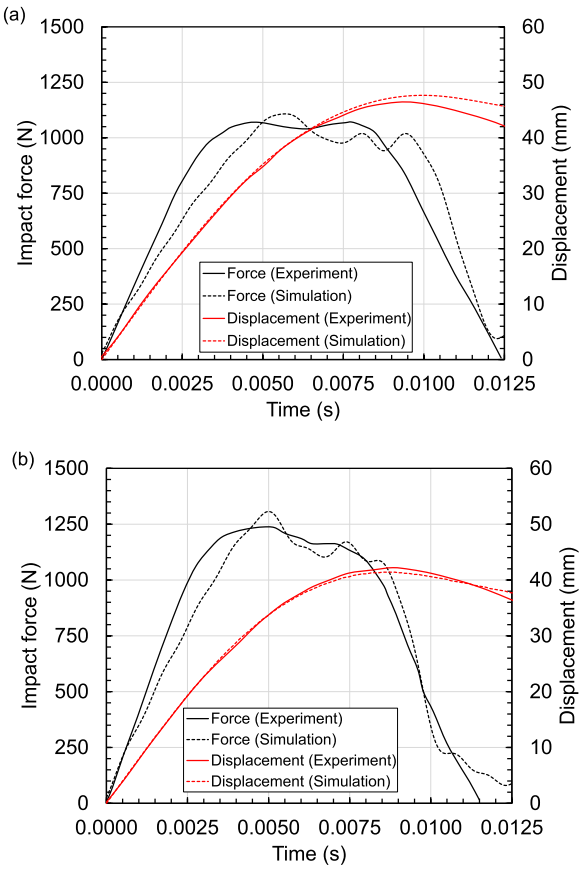

Fig. 3. Impact force and displacement time histories for the EPS foam with two densities: (a) 13.0 kg/m^3, and (b) 18.0 kg/m^3. Note that the reported displacement is for the center of the front face of the EPS foam.

assumed to be fixed, following the support conditions used in the experiments. From the simulations conducted for model validation, several response measures, including residual velocities and damage patterns, are extracted and compared to those recorded during the experiments. Table 1 provides a side-by-side comparison of the residual velocities and penetration modes. Both measures are found in agreement with those obtained from the experiments. In the current study, the first four specimens (i.e., SP1 through SP4) are utilized for model calibration, while the last two specimens (i.e., SP5 and SP6) are employed for model verification.

In addition to the comparisons reported in Table 1, the displacements at the back sheet of the SIPs are compared. In the experiments, the displacements were measured at two locations midway between the center and the two edges (i.e., long edge and short edge) of the panel. The maximum displacements recorded at these two locations were 18.9 mm and 11.4 mm for the SP4 specimen. The FE simulation provides a close approximation of 18.6 mm and 12.3 mm at the same two locations. In addition to comparing the displacements, Fig. 4 depicts the post-impact damage pattern of the SP4 specimen obtained from the experiment and FE simulation. From the deformed shape, a close agreement of the folds formed in the front sheet can be confirmed. Upon the successful completion of model validation, the base model for the DL-SIPs is created with the dimensions of 1.2 m × 2.4 m and two 50-mm thick cores. To obtain an optimum mesh size, a detailed mesh convergence analysis is conducted on the DL-SIPs. Based on the analysis results, a mesh size of 5 mm is found appropriate for the immediately impacted area. The mesh size is then increased to 20 mm for the rest of the surface area. In both areas, the depth of individual elements is 5 mm (i.e., 10 elements for a core thickness of 50 mm).

4. Impact response analysis of DL-SIPs

After validating the developed FE simulation platform, analyses are performed to first understand the effects of the middle sheet on the impact response of DL-SIPs. This is an important parameter, as it separates single-layered SIPs from double-layered ones. To make side-by-side comparisons possible, the single-layered and double-layered SIPs are assumed to have the same total mass. The single-layered SIP under consideration has a core thickness of 100 mm and a metal sheet thicknesses of 0.6 mm at the front and back. For the DL-SIP, two configurations are developed, noting that the front sheet's thickness greatly influences the penetration resistance of the panels. The first configuration has an equal thickness of 0.4 mm for the three metal sheets, whereas the second configuration has a front sheet thickness of 0.6 mm and a middle and a back sheet with a thickness of 0.3 mm each. For both single-layered and double-layered SIPs, the foam core density is assumed to be the same, i.e., 61.0 kg/m^3. The simulations are conducted for a wide range of impact velocities between 5.0 m/s to 40.0 m/s (with an increment of 2.5 m/s). Fig. 5 compares the projectile penetration depth and residual velocity curves. Comparing the single-layered and double-layered SIPs, the projectile penetration depth does not reflect a significant difference up to an impact velocity of 15.0 m/s. However, with increasing the impact velocity to 17.5 m/s, the front sheet ruptures in the single-layered SIP, as well as in the DL-SIP that has the metal sheets of equal thickness. Consequently, a sharp increase in the penetration depth is recorded in both panels. Under the same impact velocity, the DL-SIP with a front sheet of 0.6 mm resists the impact-induced forces with no damage.

In the single-layered SIP, the projectile reaches the back sheet if the initial impact velocity is 20.0 m/s. Under the same velocity, the contribution of the middle sheet in the DL-SIPs emerges, as the projectile is stopped after reaching the middle sheet. As the velocity is further increased to 25.0 m/s, only the second configuration of the DL-SIP is found to resist the projectile impact. Fig. 5(b) compares the residual velocity curves of the three panels obtained from the windborne debris impacts. With an identical front sheet, the middle sheet is observed to affect the residual velocities significantly. In terms of critical velocity, which is defined as the velocity required for a debris to penetrate into a panel with zero residual velocity, it is noted that a critical velocity of 25.8 m/s is recorded for the second configuration of the DL-SIP. This is up to 10% higher than the critical velocities obtained for the other two

Table 1
Details of the specimens considered for the validation study, along with the experimental test and numerical simulation results.

No.	Face Sheet Thickness (mm)	Core Thickness (mm)	In-Plane Dimension (m)	Debris Mass (kg)	Initial Impact Velocity (m/s)	Residual Velocity (m/s)		Perforation	
						Experiment	Simulation	Experiment	Simulation
SP1	0.4	50	0.76 × 1.20	4.0	18	−3.8	−4.5	No	No
SP2	0.4	50	0.76 × 1.20	4.0	26	17.0	17.8	Yes	Yes
SP3	0.4	50	0.76 × 1.20	4.0	23	15.0	14.1	Yes	Yes
SP4	0.4	75	0.76 × 1.20	4.0	24	10.0	11.5	Yes	Yes
SP5	0.4	75	0.76 × 1.20	4.0	18	−4.0	−4.1	No	No
SP6	0.4	38	1.40 × 1.20	4.0	18	0.0	0.0	No	No

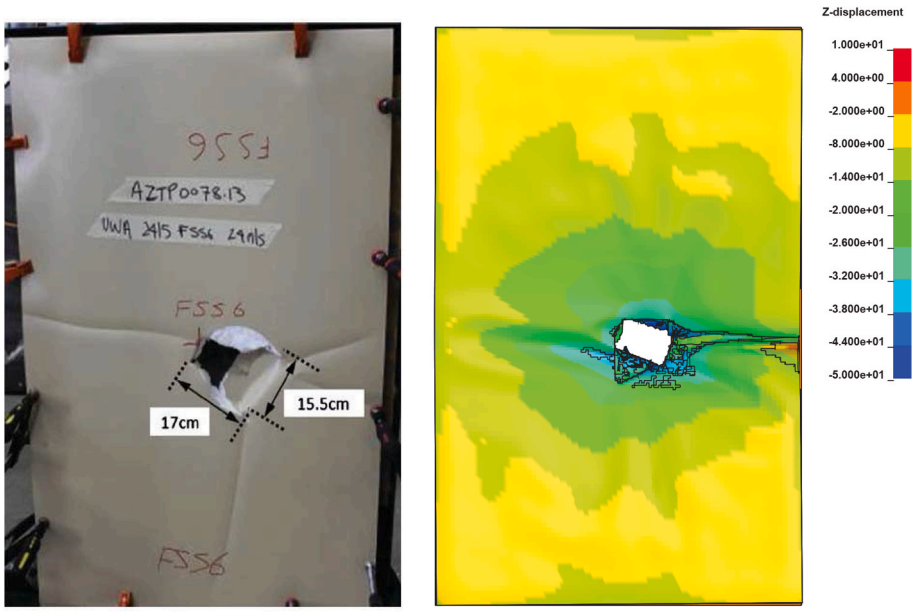

Fig. 4. Comparison of the deformed shapes of the SP4 specimen obtained from (a) the experimental test [10], and (b) the FE simulation.

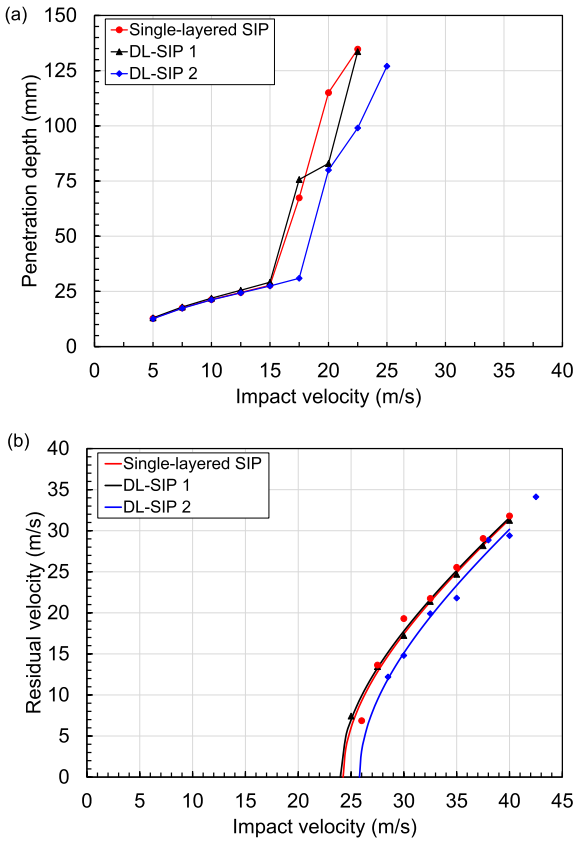

Fig. 5. Performance of the single-layered and double-layerd SIPs, in terms of (a) projectile penetration, and (b) residual velocity.

panels under consideration.

The impact resistance of the DL-SIP with equal metal sheet thicknesses of 0.4 mm is examined in detail using various response measures, such as damage pattern, energy absorption, maximum displacement, and projectile penetration. Fig. 6 shows the DL-SIP's component-based energy absorption curves extracted for the impact velocities of 15.0 m/s, 20.0 m/s, and 25.0 m/s. The DL-SIP experiences different damage patterns as the impact velocity increases. Under an impact velocity of 15.0 m/s, the panel fully resists the windborne debris with only a small deformation in the front sheet. This is through a global deformation, which is reflected in the fact that the two foam cores dissipate almost 90% of the impact-induced kinetic energy. With increasing the impact velocity to 20.0 m/s, the front metal sheet ruptures and the debris rebounds after reaching the middle metal sheet. This is accompanied by localized deformations in the front sheet and the first foam core. After the debris contacts the middle metal sheet, 6% of the kinetic energy is dissipated and the debris rebounds. However, if the impact velocity is further increased to 25.0 m/s, the DL-SIP experiences full penetration. Under this impact velocity, all the components of the DL-SIP are observed to actively participate in the energy dissipation process.

The deformation pattern is another measure employed to understand the impact response of the DL-SIP under consideration. Through monitoring the deformation contours formed under the three impact velocities of 15.0 m/s, 20.0 m/s, and 25.0 m/s (Fig. 7), punching shear is found as the primary mode of failure. Fig. 8 presents the component-based energy absorbed by the DL-SIP obtained at various impact velocities between 5.0 m/s and 40.0 m/s. For the impact velocities up to 17.5 m/s, the front sheet increasingly absorbs the impact energy. As the velocity increases further, the energy absorbed by the front sheet remains constant. As a result, a decrease in the normalized energy is reported for the front sheet. Similar observations are made for the first foam core. The middle and back sheets participate in energy dissipation when the impact velocity exceeds 20.0 m/s and 25.0 m/s, respectively. For the impact velocities greater than 25.0 m/s, both of the first and second cores absorb almost a similar amount of impact energy.

The impact response of the DL-SIP is further studied, in terms of the displacement of the panel and the penetration depth of the projectile. When the projectile impacts the DL-SIP, the panel first undergoes localized deformations followed by global deformations. Consequently, the front sheet is often displaced more than the other two sheets. Fig. 9 shows the displacement time histories for the front, middle, and back sheets of the DL-SIP under a 15 m/s impact velocity. A maximum displacement of 27.6 mm is observed for the front sheet, as compared to 22.0 mm and 21.0 mm recorded for the middle and back sheets, respectively. Fig. 10 illustrates the maximum displacement of the back

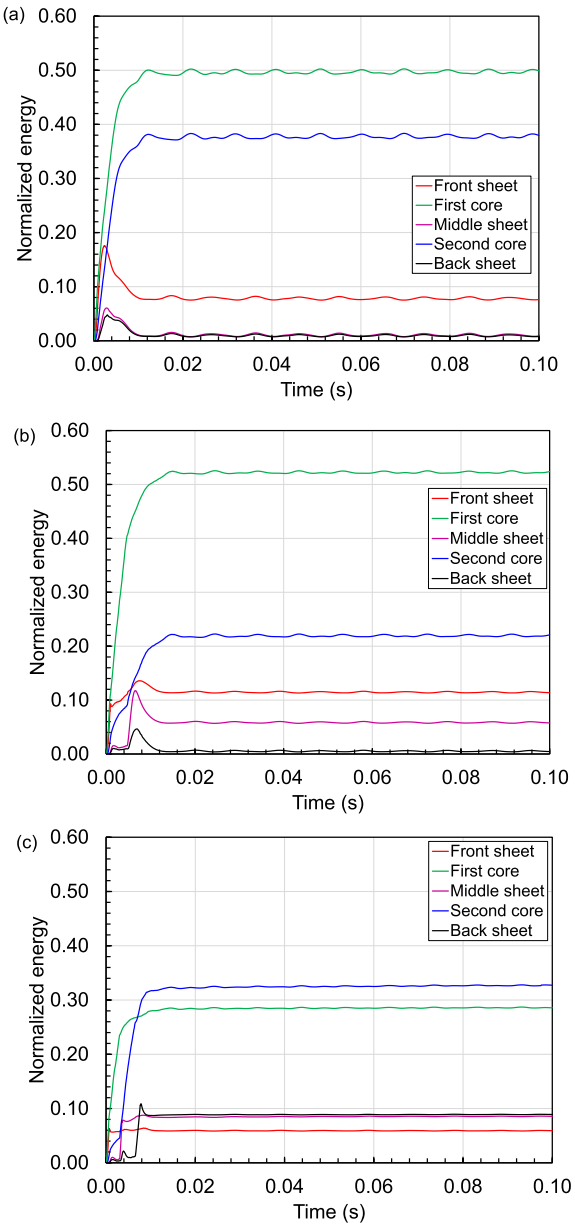

Fig. 6. Time-histories of the fractions of the total impact energy absorbed by the main components of the DL-SIPs under an impact velocity of (a) 15.0 m/s, (b) 20.0 m/s, and (c) 25.0 m/s.

sheet and the penetration depth of the windborne debris for a range of impact velocities between 5.0 m/s to 22.5 m/s (at 2.5 m/s intervals). Both measures are found to increase almost linearly for the impact velocities below 15.0 m/s. Under the impact velocity of 15.0 m/s, the projectile penetration is found to be less than 20 mm, as the DL-SIP does not undergo any notable damage. With increasing the impact velocity to 17.5 m/s, the projectile penetrates through the front metal sheet, which is characterized by a sudden increase in the penetration depth. However, the maximum displacement of the back sheet does not significantly increase under this impact velocity. As the impact velocity is further increased to 20 m/s, the projectile rebounds after reaching the middle sheet. This induces a sharp increase in the maximum displacement of the back sheet, while the projectile penetration depth witnesses only a slight increase. This can be explained by the local compression applied to the second foam core after the projectile reaches the middle sheet. When the impact velocity is further increased to 22.5 m/s, the projectile penetrates through the middle sheet, resulting in more than 60% increase in the penetration depth.

5. Investigation of main design parameters

A comprehensive analysis is performed to understand and evaluate the effects of the main DL-SIP design parameters on their response to windborne debris impact. The parameters of interest include (i) foam core density, (ii) foam core thicknesses, (iii) metal sheet thicknesses, and (iv) yield stress of metal sheets. The effects of the foam density on the response of the DL-SIPs are studied considering three foam densities of 13.5 kg/m^3, 61.0 kg/m^3, and 112.0 kg/m^3. The core density influences the elastic, plateau, and densification regions of the foam's stress-strain curve. The DL-SIPs considered for this investigation consist of 0.4-mm thick metal sheets with a yield strength of 330 MPa, as well as two EPS foam cores, each with a thickness of 50 mm. The response measures of interest are extracted from the FE simulations under a wide range of impact velocities between 5.0 m/s to 40.0 m/s (with 2.5 m/s intervals). Fig. 11 presents the maximum displacements and penetration depths of the three DL-SIPs under various impact velocities until the debris fully penetrates through the panel. The maximum displacements recorded at the back of the panels are observed to follow a complex pattern. Intuitively, the maximum displacement is expected to be reduced, as the density of the foam core in the DL-SIP increases. For the impact velocities less than 12.5 m/s, however, Fig. 11(a) shows a higher maximum displacement for the DL-SIPs with denser foam cores. This is because of a larger global deformation in the DL-SIP, as a denser foam core is used. With increasing the impact velocity to 20.0 m/s, the pattern reverses, due to the fact that the maximum displacement is governed by localized deformations, instead of global ones. The scope of the investigation on the effects of the foam core density is further extended by comparing the penetration depths obtained under different impact velocities. For the impact velocities below 12.5 m/s, an increase of 30% in the penetration depth is observed with decreasing the foam core density from 61.0 kg/m^3 to 13.5 kg/m^3. A similar change, however, is not observed with decreasing the foam core density from 112.0 kg/m^3 to 61.0 kg/m^3. In particular, beyond the impact velocity of 15.0 m/s, the foam core density's contribution becomes further prominent. This is to a level that the projectile penetration is reduced significantly when using a foam core density of 112.0 kg/m^3, which has the highest elastic modulus among the three foam cores considered in the current study.

Fig. 14(a) presents the specific energy absorption obtained from the windborne debris impact analysis of the DL-SIPs with different core densities. It must be noted that the specific energy absorption is defined as the energy absorbed per unit mass of the DL-SIPs. This measure is observed to increase with increasing the impact velocity until the panel undergoes perforation. For example, the DL-SIP with the core density of 13.5 kg/m^3 reaches its maximum specific energy absorption of 31.1 J/kg at the impact velocity of 25.0 m/s. Beyond this velocity, the specific energy absorption drops to an almost constant value. As expected, the DL-SIPs with a higher core density provide a better protection against windborne debris impact. This improvement, however, comes at the expense of significant increase in the total mass. This is properly reflected in the specific energy absorption, which decreases with increasing the core density, despite an overall increase in the total energy absorption. Up to the impact velocity of 20.0 m/s, the specific energy absorption for the DL-SIP with a core density of 61.0 kg/m^3 is recorded to be approximately 0.7 and 1.3 times of that for the DL-SIPs with the core densities of 13.5 kg/m^3 and 112.0 kg/m^3, respectively. Beyond the 25.0 m/s impact velocity, however, the windborne debris penetrates through the DL-SIPs with the core density of 13.5 kg/m^3 and 61.0 kg/m^3, resulting in an almost constant specific energy absorption. On the other hand, the specific energy absorption for the DL-SIP with the core density of 112.0 kg/m^3 increases to become higher than that for the other two DL-SIPs when the impact velocity exceeds 30.0 m/s.

To evaluate the effects of the core thickness, three total thicknesses of 100 mm, 125 mm, and 150 mm are considered, assuming an equal

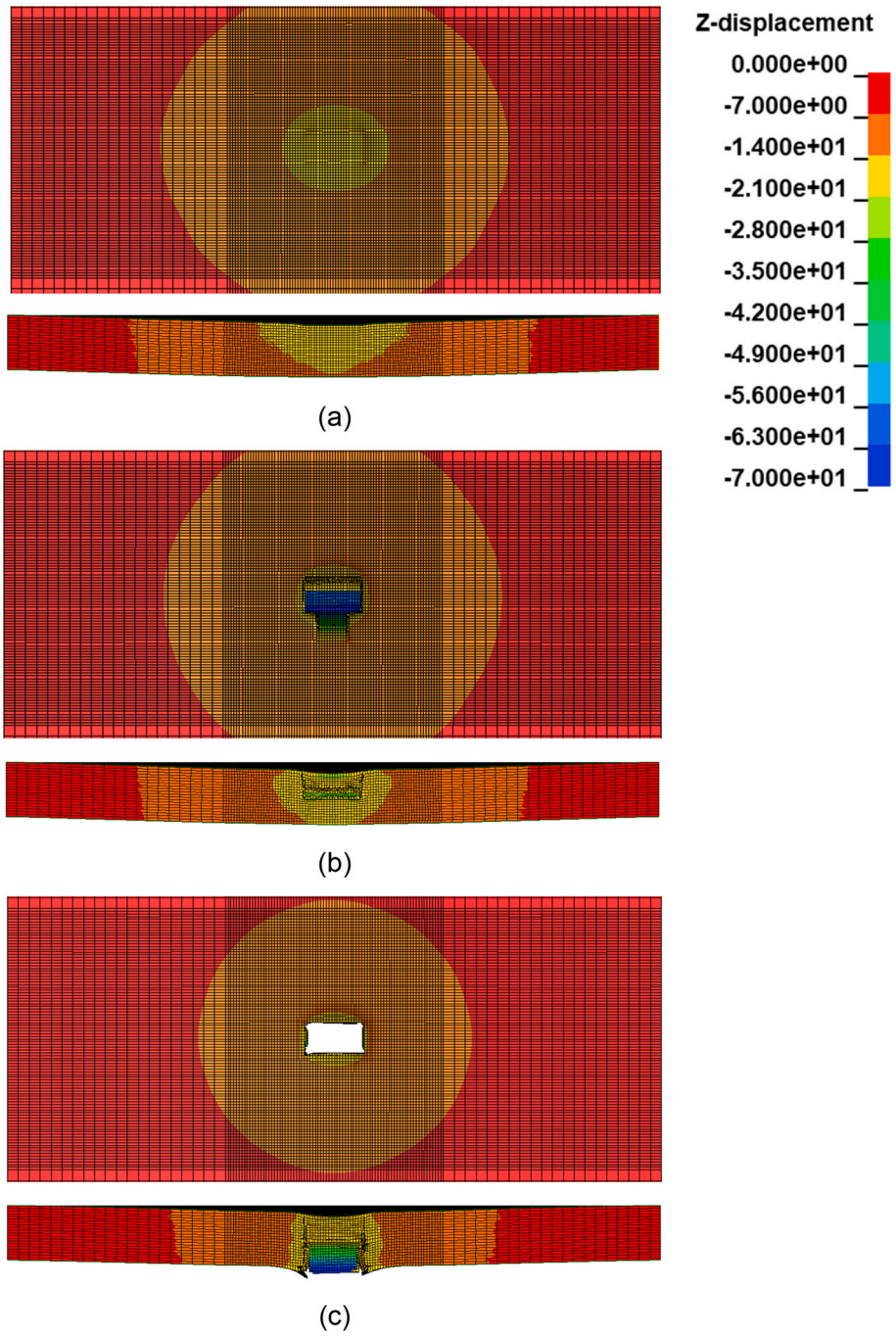

Fig. 7. Deformed shapes of the main DL-SIP under an impact velocity of (a) 15.0 m/s, (b) 20.0 m/s, and (c) 25.0 m/s.

thickness assigned to the first and second cores. The DL-SIPs consist of 0.4-mm thick metal sheets with a yield strength of 330 MPa. The foam density is considered to be 61.0 kg/m^3. Fig. 12 presents the variation of maximum displacement at the back of the panel for a range of impact velocities between 5.0 m/s and 25.0 m/s. The maximum displacement is found to decrease with increasing the core thickness. This trend becomes more pronounced under higher impact velocities. For the cores with the total thickness of 125 mm and 150 mm, the projectile penetrates through the DL-SIPs under any impact velocity beyond 25.0 m/s. This velocity is lowered to 22.5 m/s for the DL-SIP with the core's total thickness of 100 mm. The effects of the core thickness can be further explained using the specific energy absorption of the DL-SIPs, as shown in Fig. 14(b). Compared to the core density, only a slight difference in the specific energy absorption is noted with changing the total thickness of the cores. The three DL-SIPs reach their maximum specific energy absorption at the impact velocity of 25.0 m/s.

The metal sheet thickness is an important factor that can govern the penetration resistance of DL-SIPs. The effects of the metal sheet thickness are investigated by considering three thicknesses of 0.4 mm, 0.5 mm, and 0.6 mm for each sheet. Fig. 13(a) illustrates how the penetration depth changes with the change in the metal sheet thickness of the DL-SIPs that have a total thickness and density of 100 mm and 61.0 kg/m^3 for their cores, respectively. Under the velocities less than 15.0 m/s, the debris penetration depth shows a linear increasing trend with a negligible difference among the three DL-SIPs. The difference in the recorded penetration depths, however, becomes more pronounced at higher impact velocities. While the DL-SIP with a metal sheet thickness of 0.4 mm undergoes perforation at an impact velocity of 25.0 m/s, the

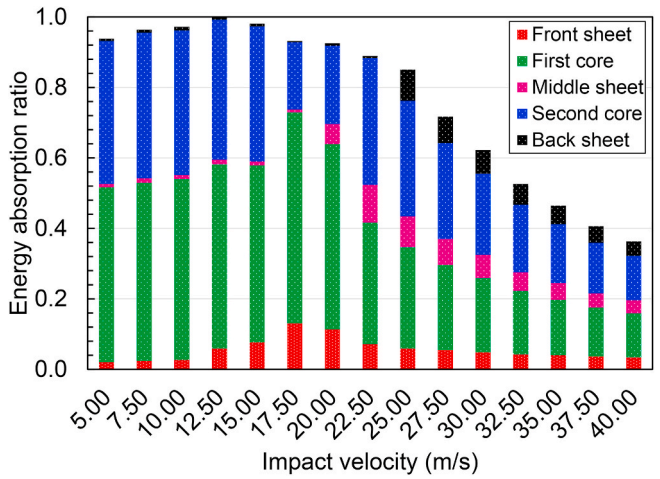

Fig. 8. Component-based energy absorption recorded in the DL-SIPs under various impact velocities.

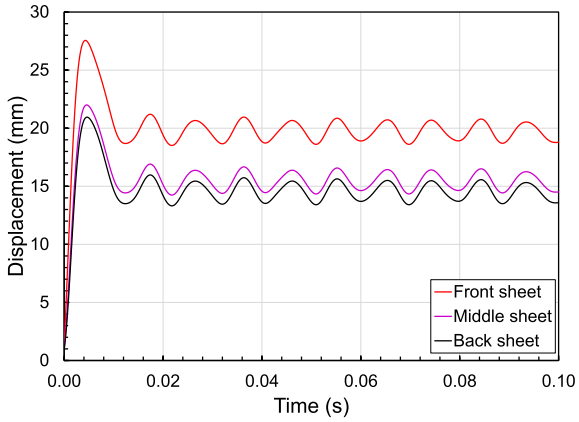

Fig. 9. Displacement time-histories of the three metal sheets of the base DL-SIP under an impact velocity of 15.0 m/s.

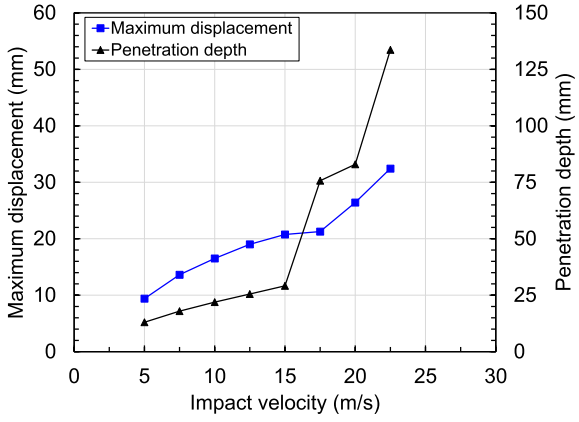

Fig. 10. Comparison of the maximum displacement at the back of the DL-SIPs and the projectile penetration under various impact velocities.

other two DL-SIPs are found to resist the impact-induced forces with no perforation under the same impact velocity. With the impact velocity of 25.0 m/s, the DL-SIPs with the metal sheet thicknesses of 0.5 mm and 0.6 mm are observed to have a penetration depth of 125.1 mm and 107.3 mm, respectively, indicating that the debris can penetrate only through the middle sheet in both DL-SIPs. If the velocity is increased to

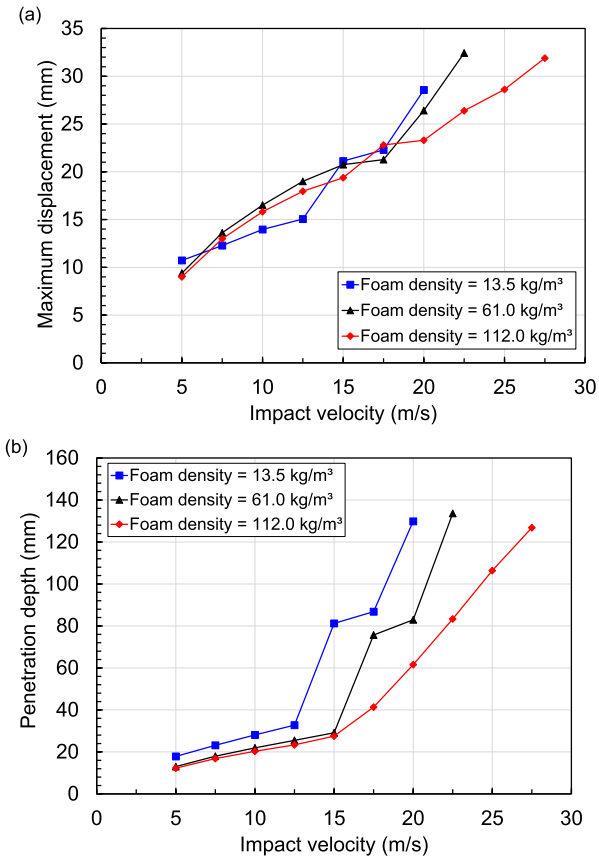

Fig. 11. Effects of foam core density on (a) maximum displacement, and (b) penetration depth.

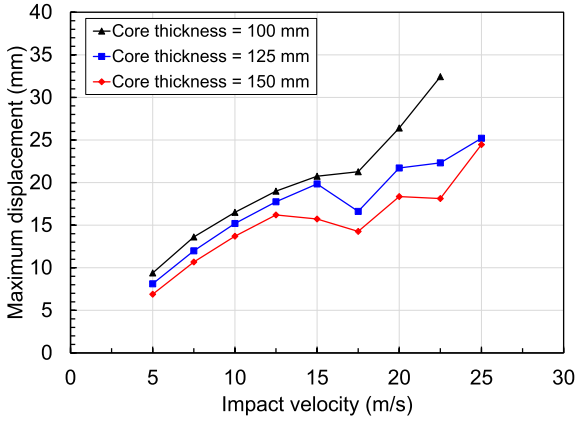

Fig. 12. Maximum displacement at the back of the DL-SIPs with different core thicknesses.

27.5 m/s, the DL-SIP with a sheet thickness of 0.5 mm cannot withstand the impact load and undergoes perforation. The DL-SIP with a sheet thickness of 0.6 mm shows the highest penetration depth, i.e., 133.5 mm, and undergoes perforation under the impact velocities higher than 27.5 m/s. The obtained responses can be further explained by monitoring the maximum specific energy absorption for the three panels, as shown in Fig. 14(c). For all the impact velocities, the energy absorption provided by the DL-SIPs increases with increasing the metal sheet thickness. This, however, is not observed for the specific energy absorption, as the change of this measure with the impact velocity becomes negligible when the impact velocity exceeds 27.5 m/s.

Further to the thickness of the metal sheets, their yield strength is

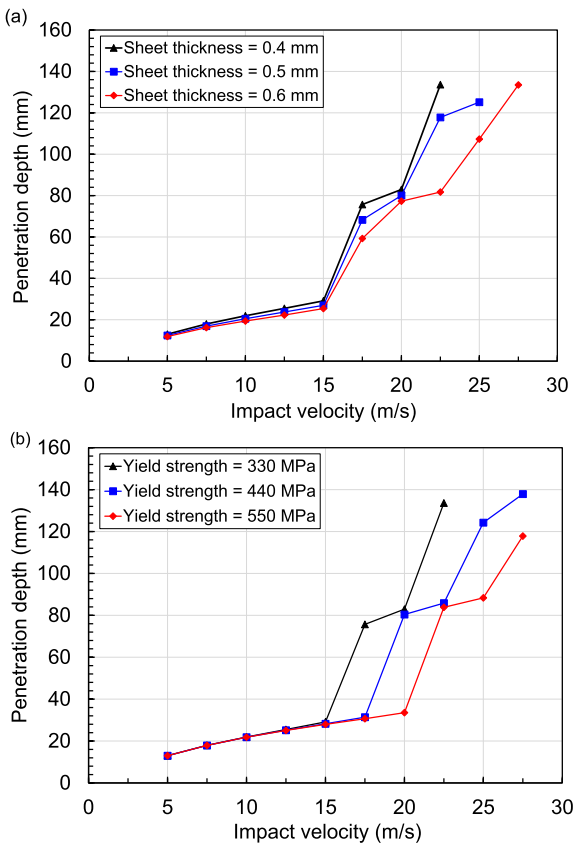

Fig. 13. Variations in the penetration depth experienced by the DL-SIPs with (a) different metal sheet thicknesses, and (b) different yield strengths of the metal sheets.

known to significantly affect the penetration resistance of the DL-SIPs. To investigate this parameter, three yield strengths of 330 MPa, 440 MPa, and 550 MPa are considered. The modeled DL-SIPs have a total core thickness of 100 mm and a core density of 61.0 kg/m^3. Fig. 13(b) shows the penetration depths obtained from the conducted simulations with various impact velocities from 5.0 m/s to 27.5 m/s. Similar penetration depths are obtained for the three panels with a linear increase as the impact velocity increases to 15.0 m/s. For the DL-SIPs with the yield strengths of 330 MPa, 440 MPa, and 550 MPa, the panel's front sheet is found to rupture under the impact velocities beyond 15.0 m/s, 17.5 m/s, and 20.0 m/s, respectively. Similar differences are observed for the rupture of the middle and back sheets among the three panels. Fig. 14(d) presents the effects of the yield strength of the metal sheets on the specific energy absorption of the DL-SIPs under a wide range of impact velocities. For the impact velocities lower than 22.5 m/s, the three panels are found to have similar specific energy absorptions. This is because the windborne debris does not penetrate through the panels at those velocities. However, a significant difference in the specific energy absorptions is noted at the impact velocities higher than 25.0 m/s. Under the impact velocity of 35.0 m/s, for example, the specific energy absorptions of the DL-SIPs with the yield strengths of 440 MPa and 550 MPa are 1.35 and 1.63 times higher than that of the DL-SIP with the yield strength of 330 MPa, respectively.

6. Multi-objective design optimization using surrogate models

For an efficient design of DL-SIPs under the windborne debris hazard, it is important to determine the best combination of design parameters related to metal sheets and foam cores. This is expected to lead to a satisfactory impact resistance without having to overdesign the panels. The detailed study presented in the previous sections reveals that the thickness of the front, middle, and back sheets, yield strength of the metal sheets, and density and thickness of the first and second foam cores are among the most influential design parameters. With the ultimate goal of delivering an optimized design for DL-SIPs, three multi-objective design optimizations (MDOs) are introduced, spanning three scenarios to capture the trade-offs among the penetration depth, maximum displacement, and specific energy absorption measures obtained for a holistic matrix of design combinations:

- MDO I: minimize the maximum displacement and maximize the specific energy absorption
- MDO II: minimize the penetration depth and maximize the specific energy absorption
- MDO III: minimize the maximum displacement, minimize the penetration depth, and maximize the specific energy absorption

Subjected to

$$0.4\ \text{mm} \le t_F,\ t_M,\ \text{and}\ t_B \le 1.0\ \text{mm}$$

$$330.0\ \text{MPa} \le \sigma_{st} \le 550.0\ \text{MPa}$$

$$13.5\ \text{kg}/\text{m}^3 \le \rho_1 \ \text{ and } \rho_2 \le 112.0\ \text{kg}/\text{m}^3$$

$$50.0\ \text{mm} \le t_{C1}\ \textit{and}\ t_{C2} \le 75.0\ \text{mm}$$

where t_F, t_M, and t_B are the thickness of the front, middle, and back sheet, respectively; σ_{st} is the yield strength of the metal sheets; ρ_1 and ρ_2 are the density of the first and second foam core, respectively; and t_{C1} and t_{C2} are the thickness of the first and second foam core, respectively. To solve the MDO problems, the formulation of the objective and constraint functions requires a large number of design iterations. To reduce the number of simulations and subsequently computational demand, surrogate models are used to perform global approximations. In this study, two surrogate models, i.e., radial basis function (RBF) network and kriging model, are employed to develop the objective response functions. For the construction of the RBF network, a Gaussian function has been used as the basis function. In addition, a cross-validation error has been employed as the optimization criterion of the RBF network [34,35]. For the kriging model, a Gaussian function has been used as the correlation function, along with a trend model, which is linear with respect to model parameters [36,37]. The training set for the surrogate models is determined by the Latin hypercube sampling (LHS) method, which has been widely used for the design of experiments. A total of 120 samples are generated over the design space. With a single-stage optimization approach, the non-dominated sorting genetic algorithm (NSGA-II) is adopted to evaluate the optimums used for solving the three MDOs, i.e., MDO I, MDO II, and MDO III, with the two surrogate models. The solutions are obtained in the form of a Pareto-optimal front, which helps determine the optimal design.

In the current study, the optimization is performed following the extreme test conditions provided in the Florida Building Code [4]. For the panels to be designed in high wind regions, the Florida Building Code [4] requires them to resist the impact of sawn lumbers weighing 4.1 kg (8.8 lb) with the velocity of 24.4 m/s (54.6 mph). The RBF network and the kriging model are each trained using the simulation results obtained for 120 combinations over the design space. The fitting accuracies of the two surrogate models are then evaluated using the R^2 and RMS error, while the prediction accuracies of the surrogate models are validated with another 10 design combinations not originally used. Among the three key impact response measures, i.e., penetration depth, maximum displacement, and specific energy absorption, the RBF network delivers the best approximation for specific energy absorption with the R^2 and RMS error of 0.99 and 1.15%, respectively, while it predicts the maximum displacement with the R^2 and RMS error of 0.83 and 5.43%, respectively. On the other hand, the kriging model has the R^2

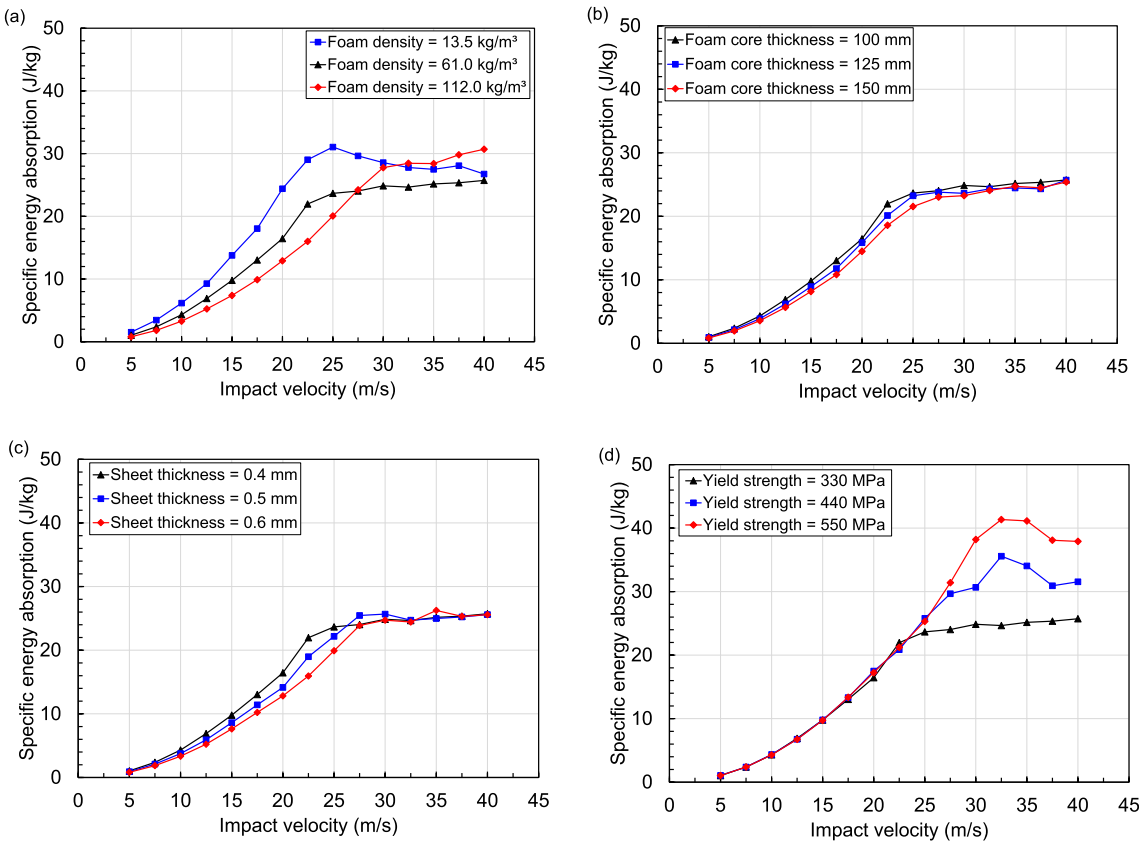

Fig. 14. Effects of various design variables on the specific energy absorption of the DL-SIPs: (a) density of the foam core, (b) thickness of the foam core, (c) front sheet thickness, and (d) yield strength of the metal sheets.

value of 0.99 for the approximation of all the three response measures. This suggests that the kriging model can be employed to approximate the impact response of DL-SIPs very well.

6.1. Global sensitivity analyses

To understand and quantify the significance of the main design parameters, surrogate model-based global sensitivity analyses are conducted with a primary focus on variations in the key impact response measures of DL-SIPs. In this study, the Sobol method [38] is employed to evaluate the sensitivity of the penetration depth, maximum displacement, and specific energy absorption to individual design variables, such as thickness of the front, middle, and back metal sheets, yield strength of the metal sheets, and density and thickness of the first and second foam cores. In the absence of analytical functions, the developed kriging model is used to perform the sensitivity analyses. In the sensitivity analyses, the higher order estimators are considered. However, their contributions are found negligible. The Sobol's index, S_i, of a design variable, V_i, is computed as follows:

$$S_i = \frac{\text{variance caused by } V_i}{\text{total variance of response}} \tag{8}$$

The sum of all the Sobol's indices obtained for a given response measure must be equal to one. Fig. 15 shows the percentage of contribution of the investigated design variables to the impact response characteristics of the DL-SIPs. The maximum displacement is found to be mainly dependent on the front sheet thickness, yield strength of the metal sheets, and density of the two foam cores, with a combined contribution of 82.0%. The front sheet thickness contributes to 28.2% of the total response, followed by the yield strength of the metal sheets with a contribution of 16.8%. The bottom sheet thickness also contributes 5.4% to the maximum displacement. Other design variables, such as

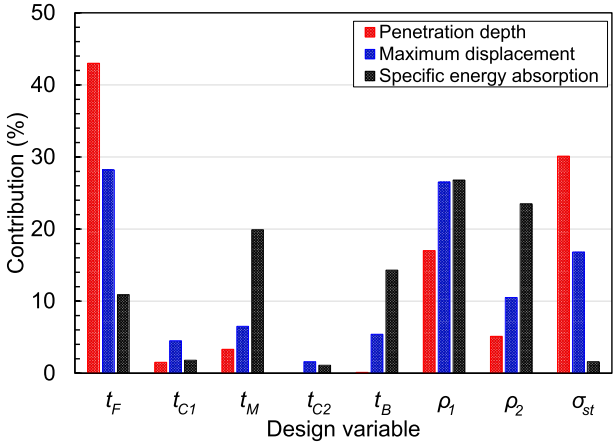

Fig. 15. Sobol's indices of the main design variables obtained for the impact response of the DL-SIPs over the design space.

core thickness and the thickness of the middle sheet, are determined to be less consequential. The design variables are found to affect the penetration depth similar to how they influence the maximum displacement. This is, however, with a slightly higher contribution from the front sheet thickness and the yield strength of the metal sheets. The front sheet thickness, yield strength of steel, and first core density contribute to almost 90% of the total response combined. From these contributions, it can be inferred that the debris impact resistance of the DL-SIPs can be improved by increasing the front sheet thickness, yield strength of the employed steel, and density of the first foam core.

Next, the effect of the main design variables on the specific energy

absorption is studied. From the Sobol's indices, several design variables influence the specific energy absorption of DL-SIPs. The density of the foam cores have a major influence with a total contribution of 50.3%. In addition to the foam cores, the metal sheet thicknesses contribute to 45.1% of the total response. Among the three metal sheets, the specific energy absorption is found most sensitive to the middle sheet thickness with a contribution of 19.9%. This highlights the importance of the middle sheet in absorbing the impact-induced energy. The detailed information reported in this section reflects how the size and material proprieties of the DL-SIPs contribute to the impact response of this important category of wall panels. However, an optimized design can only be achieved with the proper selection of all the introduced parameters. This has motivated a rigorous multi-objective optimization study, as presented in the next section.

6.2. Design optimization

The current study considers three MDOs, i.e., MDO I, MDO II, and MDO III. The solution for MDO III is a combination of MDO I and MDO II. However, the solution for MDO I and MDO II cannot be necessarily obtained from MDO III. Based on the introduced surrogate models, the Pareto-optimal fronts of the first two MDOs are developed, as shown in Fig. 16. For these two optimizations, the predictions of the Pareto-optimal fronts are found relatively close to each other. As reflected in Fig. 16(a), the maximum displacement decreases with increasing the specific energy absorption. On the other hand, Fig. 16(b) illustrates how the penetration depth can be minimized by increasing the specific energy absorption. From the obtained Pareto-optimal fronts, a set of configurations are selected for each of the MDOs. Table 2 through 4 presents

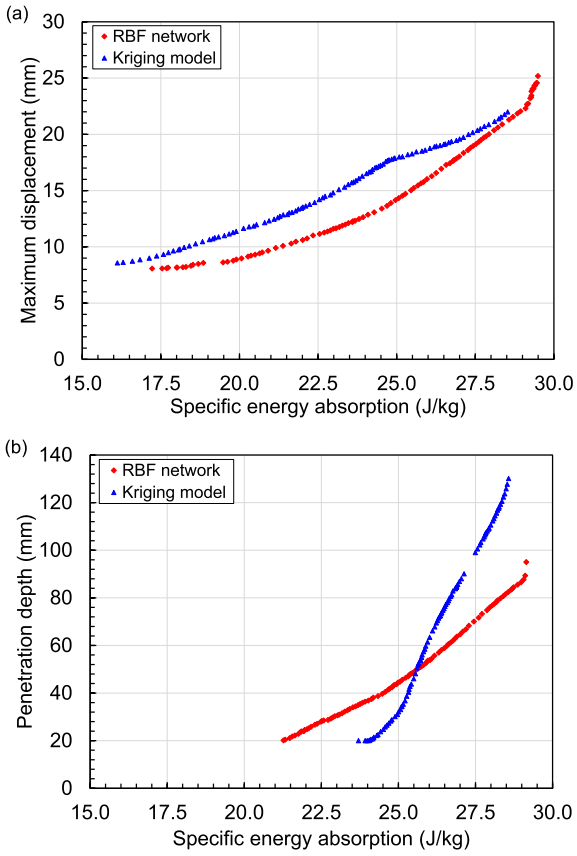

Fig. 16. Pareto-optimal front of the DL-SIPs for the two surrogate models: (a) minimize the maximum displacement and maximize the specific energy absorption, and (b) minimize the penetration depth and maximize the specific energy absorption.

the five configurations of the DL-SIPs for each of the three MDOs obtained using the kriging model.

The design configurations of the DL-SIPs selected to reduce the maximum displacement and enhance the energy absorption capacity are summarized in Table 2. From this table, a (relatively) thick front sheet, along with thick foam cores, are found effective in reducing the maximum displacement. From the design configurations considered, the EPS foam with a density of (at least) 16.2 kg/m^3 is found necessary for the first core to meet the design objectives. For achieving the two objectives of minimizing the projectile penetration and maximizing the specific energy absorption, five design configurations are provided in Table 3. It is evident in this table that a thick front sheet with a steel yield strength of 550 MPa can be appropriate to minimize the projectile penetration depth. Contrary to the design configurations targeted to minimize the maximum displacement, a foam core thicknesses of 50 mm is sufficient for minimizing the projectile penetration. Foam cores with a density of 14.0 kg/m^3 is also deemed satisfactory for the design of DL-SIPs. Table 4 provides the design configurations for the three objectives of minimizing the maximum displacement and projectile penetration, while maximizing the specific energy absorption. To meet these design objectives at the same time, the DL-SIPs must be designed with a (relatively) thick front sheet that has a high yield strength, in addition to using thick foam cores. A higher foam density considered for the first core also leads to a lower maximum displacement and projectile penetration.

7. Conclusions

This study provided a holistic investigation of DL-SIPs, as an important class of composite wall panels, under the windborne debris hazard. For this purpose, explicit dynamic simulations were conducted, capturing a wide range of impact velocities. After validating the developed FE simulation platform using the experimental test results, various DL-SIP structural response measures, including damage pattern, energy absorption, and maximum displacement, were determined and compared based on the geometric and material properties commonly used in the DL-SIPs. In the absence of any similar studies, a surrogate model-based multi-objective design optimization was then performed to identify the optimum configurations of the DL-SIPs, taking into consideration the contribution of their main design variables. The main findings and conclusions drawn from this study are as follows:

- From comparing the impact response of the DL-SIPs to that of the single-layered SIPs of the same total mass, the middle sheet was determined to reduce the projectile penetration by 25%, especially at high impact velocities. This increased resistance also resulted in an increase in the critical velocity. This highlighted how a transition from a single-layer to a double-layer configuration can contribute to achieving an improved impact resistance of the wall panels without requiring any additional materials.
- For the performance assessment of the DL-SIPs under windborne debris impact, three responses measures, i.e., projectile penetration, maximum displacement, and specific energy absorption were investigated. It was found that the projectile penetration and maximum displacement increase with increasing the impact velocity. This trend continues until the projectile ruptures the metal sheets. Under the impact velocities less than 15.0 m/s, up to 90% of the kinetic energy was determined to be absorbed by the front sheet and two foam cores. The middle and the back sheet participated in the energy dissipation process after a rupture occurred in the front sheet.
- Considering that an impact-resistant design of DL-SIPs requires an in-depth understanding of the contribution of various design parameters, this study systematically investigated the thickness and yield strength of the metal sheets, as well as the density and thickness of the first and second foam cores. The foam core density, metal sheet

Table 2
Optimal design configurations for MDO I.

Metal Sheet Properties				Foam Core Properties				Response Measure		
t_F(mm)	t_M(mm)	t_B(mm)	σ_M(MPa)	ρ_1(kg/m^3)	ρ_2(kg/m^3)	t_{C1}(mm)	t_{C2}(mm)	Maximum Displacement (mm)	Specific Energy Absorption (J/kg)	Penetration Depth (mm)
0.46	0.49	0.41	460.9	20.1	14.0	53.9	73.3	19.4	26.7	133.9
0.85	0.40	0.40	547.6	16.2	14.0	50.5	50.1	17.6	24.7	27.5
0.87	0.50	0.41	547.9	18.4	14.0	56.6	54.8	15.5	23.5	21.9
0.86	0.77	0.44	546.0	18.4	14.0	63.4	73.9	11.9	20.5	20.3
0.90	0.88	0.99	545.0	25.2	14.3	67.0	74.8	8.6	16.1	20.4

Table 3
Optimal design configurations for MDO II.

Metal Sheet Properties				Foam Core Properties				Response Measure		
t_F(mm)	t_M(mm)	t_B(mm)	σ_M(MPa)	ρ_1(kg/m^3)	ρ_2(kg/m^3)	t_{C1}(mm)	t_{C2}(mm)	Penetration Depth (mm)	Specific Energy Absorption (J/kg)	Maximum Displacement (mm)
0.42	0.40	0.40	457.8	14.0	14.0	50.1	50.2	130.2	28.6	28.1
0.43	0.40	0.40	526.2	14.0	14.0	50.1	50.1	102.2	27.6	22.7
0.59	0.40	0.40	548.4	14.0	14.0	50.1	50.2	72.3	26.3	22.5
0.68	0.40	0.40	548.1	14.0	14.0	50.1	50.2	54.1	25.7	21.2
0.76	0.40	0.40	547.3	14.0	14.0	50.1	50.1	38.7	25.3	19.3

Table 4
Optimal design configurations for MDO III.

Metal Sheet Properties				Foam Core Properties				Response Measure		
t_F(mm)	t_M(mm)	t_B(mm)	σ_M(MPa)	ρ_1(kg/m^3)	ρ_2(kg/m^3)	t_{C1}(mm)	t_{C2}(mm)	Maximum Displacement (mm)	Penetration Depth (mm)	Specific Energy Absorption (J/kg)
0.46	0.40	0.40	454.8	15.5	14.1	51.8	51.9	21.5	129.7	28.3
0.61	0.40	0.41	548.7	14.2	14.0	50.3	51.4	22.2	67.9	26.1
0.83	0.41	0.40	545.4	18.7	14.2	59.5	50.3	17.0	28.9	24.3
0.87	0.69	0.41	547.6	16.9	14.1	58.7	72.3	12.7	20.2	21.3
0.93	0.50	0.65	539.9	104.3	15.3	69.4	73.5	12.1	20.0	16.6

thickness, and yield strength of the metal sheets were found to increase the penetration resistance of the DL-SIPs. However, the specific energy absorption decreased with increasing the foam core density and the metal sheet thickness under the impact velocities less than 25.0 m/s. While the foam core thickness was determined to only marginally affect the specific energy absorption of the DL-SIPs, the effect of the foam core thickness on the maximum displacement was pronounced. With increasing the core thickness by 50 mm, the maximum displacement decreased by 45%. As for the metal sheets, increasing the yield strength provided similar specific energy absorptions when the debris did not penetrate through the DL-SIPs. When the perforation occurred, however, the specific energy absorption increased by 63% with using the metal sheets that had the yield strength of 550 MPa instead of 330 MPa.

- The impact simulation results were paired with a set of global sensitivity analyses to quantify the influence of the main design parameters on the impact response of DL-SIPs. For this purpose, the Sobol's method was employed. The front sheet thickness, density of the two foam cores, and yield strength of the metal sheets were determined to majorly affect the maximum displacement of the DL-SIPs. Their penetration resistance, however, was mainly influenced by the front sheet thickness and the yield strength of the metal sheets, accounting for a total contribution above 80%. In contrast to the maximum displacement and projectile penetration, the specific energy absorption was significantly affected by the middle and back sheet thicknesses. This further explained how a double-layer configuration helps with resisting the impact-induced loads.
- For an efficient design of DL-SIPs, a multi-objective design optimization was performed, considering a wide range of design variables under three optimization scenarios. In the absence of any closed-form solutions, two surrogate models, i.e., RBF network and kriging model, were employed to approximate the impact responses. Compared to the RBF network, the kriging model was found to better approximate the maximum displacement, penetration depth, and specific energy absorption. From the MDO results, a thick high-strength front sheet in combination with a thick foam core was determined to effectively reduce the maximum displacement. On the other hand, a thick high-strength front sheet was deemed sufficient to reduce the projectile penetration depth. Such wall configurations help save on materials (and their associated costs), while ensuring that the performance expectations are properly met.

Author contributions statement

Dikshant Saini: Methodology, Software, Validation, Investigation, Writing – original draft. Behrouz Shafei: Conceptualization, Methodology, Investigation, Writing – review & editing, Supervision, Funding acquisition.

Declaration of competing interest

The authors declare that they have no known competing financial interests or personal relationships that could have appeared to influence the work reported in this paper.

Acknowledgement

The research study, results of which reported in this manuscript, was partially sponsored by the National Science Foundation (NSF) under Grants No. 1826356 and 1827774. The authors would like to

acknowledge and thank the sponsor for this support. Opinions, findings, and conclusions expressed in this manuscript are of the authors and do not necessarily reflect those of the NSF.

References

[1] ICC (International Code Council). ICC/NSSA Standard for residential construction in high-wind regions. ICC 500. Country Club Hills. IL: ICC; 2014.
[2] FEMA P-361. Safe rooms for tornadoes and hurricanes: guidance for community and residential safe rooms. Washington, DC: Third Edit. FEMA.; 2015.
[3] NRC (Nuclear Regulatory Commission). Design-basis tornado and tornado missiles for nuclear power plants, vol. 1. Washington, DC: FEMA; 2007.
[4] FBC (Florida Building Commision). Florida building Code. sixth ed.. 2017. Tallahassee, FL.
[5] Chen W, Hao H. Performance of structural insulated panels with rigid skins subjected to windborne debris impacts–Experimental investigations. Construct Build Mater 2015;77:241–52.
[6] Meng Q, Hao H, Chen W. Laboratory test and numerical study of structural insulated panel strengthened with glass fibre laminate against windborne debris impact. Construct Build Mater 2016;114:434–46.
[7] Hao H, Chen W, Chen S, Meng Q. Finite element analysis of structural insulated panel with OSB skins against windborne debris impacts. Buenos-Aires, Argentina: 1st Pan-American Congr. Comput. Mech.; 2015.
[8] Saini D, Shafei B. Vulnerability of metal roof decking systems subjected to windborne debris impact. FL: 5th Am. Assoc. Wind Eng. Work. Miami; 2018.
[9] Chen W, Hao H, Li J. Fragility curves for corrugated structural panel subjected to windborne debris impact. Int. Conf. Performance-based Life-cycle Struct. Eng. 2015:877–83.
[10] Chen W, Hao H. Experimental and numerical study of composite lightweight structural insulated panel with expanded polystyrene core against windborne debris impacts. Mater Des 2014;60:409–23.
[11] Meng Q, Hao H, Chen W. Experimental and numerical study of basalt fibre cloth strengthened structural insulated panel under windborne debris impact. J Reinforc Plast Compos 2016;35:1302–17.
[12] Saini D, Shafei B. Performance of structural insulated panels with metal skins subjected to windborne debris impact. Compos B Eng 2020;198:1–12. 108163.
[13] Marom I, Bodner SR. Projectile perforation of multi-layered beams. Int J Mech Sci 1979;21:489–504.
[14] Zhou DW, Stronge WJ. Ballistic limit for oblique impact of thin sandwich panels and spaced plates. Int J Impact Eng 2008;35:1339–54.
[15] Jing L, Yang F, Zhao L. Perforation resistance of sandwich panels with layered gradient metallic foam cores. Compos Struct 2017;171:217–26.
[16] Sun G, Wang E, Wang H, Xiao Z, Li Q. Low-velocity impact behaviour of sandwich panels with homogeneous and stepwise graded foam cores. Mater Des 2018;160:1117–36.
[17] Shobeiri V. Design optimization of sandwich panels under impact loads. Eng Optim 2020:1–19.
[18] Sun G, Chen D, Wang H, Hazell PJ, Li Q. High-velocity impact behaviour of aluminium honeycomb sandwich panels with different structural configurations. Int J Impact Eng 2018;122:119–36.
[19] Palomba G, Epasto G, Crupi V, Guglielmino E. Single and double-layer honeycomb sandwich panels under impact loading. Int J Impact Eng 2018;121:77–90.
[20] Najafi M, Eslami-Farsani R. Design and characterization of a multilayered hybrid cored-sandwich panel stiffened by thin-walled lattice structure. Thin-Walled Struct 2021;161:107514.
[21] LS-DYNA. User's guide release 15.0. 2014. USA.
[22] Saini D, Shafei B. Performance of concrete-filled steel tube bridge columns subjected to vehicle collision. J Bridge Eng 2019;24(8):1–13.
[23] Saini D, Shafei B. Investigation of concrete-filled steel tube beams strengthened with CFRP against impact loads. Compos Struct 2019;208:744–57.
[24] Saini D, Shafei B. Prediction of extent of damage to metal roof panels under hail impact. Eng Struct 2019;187:362–71.
[25] Oppong K, Saini D, Shafei B. Vulnerability assessment of bridge piers damaged in barge collision to subsequent hurricane events. J Bridge Eng 2020;25(8):04020051.
[26] Oppong K, Saini D, Shafei B. Characterization of impact-induced forces and damage to bridge superstructures due to over-height vehicle collision. Eng Struct 2021;236:1–13. 112014.
[27] Cowper G, Symonds P. Strain-hardening and strain-rate effects in the impact loading of cantilever beams. Brown Univ., Div. of Appl. Mech. No. 1957;28.
[28] Avalle M, Belingardi G, Ibba A. Mechanical models of cellular solids: parameters identification from experimental tests. Int J Impact Eng 2007;34:3–27.
[29] Chen W, Hao H, Hughes D, Shi Y, Cui J, Li Z-X. Static and dynamic mechanical properties of expanded polystyrene. Mater Des 2015;69:170–80.
[30] Ouellet S, Cronin D, Worswick M. Compressive response of polymeric foams under quasi-static, medium and high strain rate conditions. Polym Test 2006;25:731–43.
[31] Saini D, Shafei B. Damage assessment of wood frame shear walls subjected to lateral wind load and windborne debris impact. J Wind Eng Ind Aerod 2020;198:1–13. 104091.
[32] Saini D, Shafei B. Concrete constitutive models for low velocity impact simulations. Int J Impact Eng 2019;132:1–13. 103329.
[33] Zhang B, Zhang X, Wu S, Zhang H. Indentation of expanded polystyrene foams with a ball. Int J Mech Sci 2019;161:105030.
[34] Song X, Sun G, Li Q. Sensitivity analysis and reliability based design optimization for high-strength steel tailor welded thin-walled structures under crashworthiness. Thin-Walled Struct 2016;109:132–42.
[35] Huang Z, Wang C, Chen J, Tian H. Optimal design of aeroengine turbine disc based on kriging surrogate models. Comput Struct 2011;89:27–37.
[36] Matheron G. Principles of geostatistics. Econ Geol 1963;58:1246–66.
[37] Kleijnen JPC. Kriging metamodeling in simulation: a review. Eur J Oper Res 2009;192:707–16.
[38] Sobol IM. Global sensitivity indices for nonlinear mathematical models and their Monte Carlo estimates. Math Comput Simulat 2001;55:271–80.